Inhibition of Dog and Human Gastric Lipases by Enantiomeric Phosphonate Inhibitors: A Structure−Activity Study

Nabil Miled,[‡,§] Alain Roussel,[§,||] Cécile Bussetta,[‡,||] Liliane Berti-Dupuis,[‡] Mireille Rivière,[‡] Gérard Buono,[⊥] Robert Verger,[‡] Christian Cambillau,*[,||] and Stéphane Canaan*[,‡,||]

Architecture et Fonction des Macromolécules Biologiques, AFMB UMR CNRS 6098, 31 Chemin Joseph Aiguier, 13402 Marseille Cedex 20, France, Laboratoire de Lipolyse Enzymatique, CNRS UPR 9025, 31 chemin Joseph Aiguier, 13402 Marseille Cedex 20, France, and ENSSPICAM UMR CNRS 6516 "Synthèse, Catalyse, Chiralité", Avenue Escadrille Normandie-Niemen, 13397 Marseille Cedex 13, France

Received June 4, 2003; Revised Manuscript Received August 12, 2003

ABSTRACT: The crystal structures of gastric lipases in the apo form [Roussel, A., *et al*. (1999) *J. Biol. Chem. 274*, 16995−17002] or in complex with the (R_P)-undecyl butyl phosphonate [$C_{11}Y_4(+)$] [Roussel, A., *et al*. (2002) *J. Biol. Chem. 277*, 2266−2274] have improved our understanding of the structure−activity relationships of acid lipases. In this report, we have performed a kinetic study with dog and human gastric lipases (DGL and HGL, respectively) using several phosphonate inhibitors by varying the absolute configuration of the phosphorus atom and the chain length of the alkyl/alkoxy substitutents. Using the two previously determined structures and that of a new crystal structure obtained with the other (S_P)-phosphonate enantiomer [$C_{11}Y_4(-)$], we constructed models of phosphonate inhibitors fitting into the active site crevices of DGL and HGL. All inhibitors with a chain length of fewer than 12 carbon atoms were found to be completely buried in the catalytic crevice, whereas longer alkyl/alkoxy chains were found to point out of the cavity. The main stereospecific determinant explaining the stronger inhibition of the S_P enantiomers is the presence of a hydrogen bond involving the catalytic histidine as found in the DGL−$C_{11}Y_4(-)$ complex. On the basis of these results, we have built a model of the first tetrahedral intermediate corresponding to the tristearoyl−lipase complex. The triglyceride molecule completely fills the active site crevice of DGL, in contrast with what is observed with other lipases such as pancreatic lipases which have a shallower and narrower active site. For substrate hydrolysis, the supply of water molecules to the active site might be achieved through a lateral channel identified in the protein core.

Organic phosphonates and phosphates are efficient inhibitors of phospholipases (*3*, *4*) and lipases (*5*−*11*). Phosphonate inhibitors have been frequently used to investigate the lipolysis mechanism since lipases have been found to undergo a conformational change from an inactive (closed) to an active (open) form upon interfacial binding. This change involves the displacement of a lid domain that blocks the access to the active site in its closed (inactive) form (*2*, *9*, *12*−*15*). The crystal structures of *Rhizomucor miehei* lipase (Rml)[1] inhibited with diethyl *p*-nitrophenyl phosphate (E_{600}) (*12*) or with *n*-hexyl phosphonate ethyl ester (*13*) established that the covalently bound inhibitors mimic the configuration and charge distribution of the first transition state in triglyceride hydrolysis. In both complexes, the phosphorus atom of the inhibitor is covalently bound to the nucleophilic Oγ of the catalytic serine. The conformations of the inhibitor chains accommodated in the catalytic crevice can suggest a binding mode for a triacylglycerol molecule in the active site.

A key point for understanding the enantioselectivity of lipases toward inhibitors or substrates is the determination of the specific interactions between each enantiomer and the side chain residues of the amino acids belonging to the lipase active site. Since 1992, several crystal structures of lipases in complex with enantiomerically pure inhibitors (*12*−*14*), acylglycerol analogues (*9*), or a racemic mixture of inhibitors (*15*) were obtained, providing some clues about the mechanism of enantio recognition by lipases.

As far as digestive lipases are concerned, E_{600} was found to be an efficient inhibitor of porcine pancreatic lipase in the presence of colipase and mixed E_{600}/bile salts micelles (*16*−*18*). Lately, it was shown that E_{600} inactivates not only pancreatic lipases, via a stoichiometric reaction, but also gastric lipases (*6*). A series of chiral organo phosphonate compounds were therefore synthesized, and their efficiency as inactivators of gastric and pancreatic lipases was studied on the basis of the nature of the leaving group and of the substituents coordinated to the phosphorus atom (*8*, *10*). In view of assessing the stereoselectivity of digestive lipases, Cavalier *et al*. (*10*) have synthesized alkyl phosphonate inhibitors where the phosphorus atom is coordinated to a leaving nitrophenyl group and variable alkyl (C) and alkoxy

* To whom correspondence should be addressed. C.C.: fax, 33.491.16.45.36; e-mail, cambillau@afmb.cnrs-mrs.fr. S.C.: fax, 33.491.71.58.57; e-mail, stephane.canaan@afmb.cnrs-mrs.fr.

‡ CNRS UPR 9025.

§ These authors contributed equally to this work.

|| AFMB UMR CNRS 6098.

⊥ ENSSPICAM UMR CNRS 6516 "Synthèse, Catalyse, Chiralité".

[1] Abbreviations: DGL, dog gastric lipase; HGL, human gastric lipase; HPL, human pancreatic lipase; Rml, *Rhizomucor miehei* lipase; β-OG, β-octyl glucoside; E_{600}, diethyl *p*-nitrophenyl phosphate; NaTDC, sodium taurodeoxycholate.

10.1021/bi034964p CCC: $25.00
Published on Web 09/20/2003

(Y) substituents with chains lengths of 1−16 carbon atoms. The racemic phosphonate compounds were synthesized and the two enantiomers of each phosphonate molecule separated on a chiral HPLC column into fastly and slowly eluted enantiomers. Their capacity to inactivate digestive lipases as human gastric and human pancreatic lipases (HGL and HPL, respectively) was assessed using the monomolecular film technique (*10*).

The first crystal structure of a digestive lipase in complex with a phosphonate inhibitor was that of HPL in complex with a racemic mixture of the methoxy undecyl phosphonate (*15*). Both enantiomers were observed in the active site of the lipase and show interactions with the two residues of the oxyanion hole. The methoxy oxygen of only one enantiomer was within hydrogen bonding distance of the $N\epsilon_2$ atom of the catalytic histidine. The C_{11} alkyl chains of both enantiomers were lying in hydrophobic grooves. Besides the covalent bond with the catalytic serine, the conformation of the inhibitor inside the catalytic pocket was due to interactions with hydrophobic side chains of the active site together with hydrogen bonding to the oxyanion hole and to the catalytic histidine. Among the phosphonate inhibitors mentioned above, the (+) enantiomer of the undecyl butyl phosphonate [$C_{11}Y_4(+)$] was cocrystallized with dog gastric lipase (DGL) which allowed the crystal structure of a gastric lipase in its open form to be obtained for the first time (*2*).

In this report, the crystal structure of DGL in complex with the (−) enantiomer of the undecyl butyl phosphonate [$C_{11}Y_4(-)$] is described in parallel with inhibition studies in the presence of a series of phosphonate compounds. On the basis of kinetic studies, as well as on the comparison of the two available crystal structures of the open gastric lipase, its enantio preference is discussed. Furthermore, these two three-dimensional structures allowed us to model the interactions with a series of phosphonate inhibitors and to propose a model for a bound physiological substrate in the active site of gastric lipases.

EXPERIMENTAL PROCEDURES

Lipase Production and Purification. The recombinant DGL was produced in transgenic maize and purified as described previously (*2*), whereas the recombinant HGL was produced in the baculovirus insect cell system and purified as described by Canaan *et al*. (*19*).

Gastric Lipase Activity Measurement. The DGL and HGL activity was measured potentiometrically at pH 5.5 and 37 °C, using the pH-stat method and the short chain triacylglycerol as a substrate (tributyrin) under the conditions established by Gargouri *et al*. (*20*). One unit of lipase activity is the amount of enzyme which catalyzes the release of 1 μmol of fatty acid per minute.

Inhibition of Gastric Lipase by Alkyl Phosphonates. Inhibition of DGL was carried out at a molar excess of inhibitor to DGL of 50 in the presence of β-octyl glucoside (β-OG at a final concentration of 40 mM) or sodium taurodeoxycholate (NaTDC at a final concentration of 10 mM). When alkyl phosphonates were used at a molar excess of 500, concentrations as high as 40 mM in NaTDC and 100 mM in β-OG were required to solubilize the inhibitors. After the chloroform was evaporated, the inhibitor was dissolved in 2-propanol at a final concentration of 4% (w/w), and β-OG or NaTDC and DGL or HGL (at a final concentration of 57 μM) were then added. Residual lipase activity was measured at various incubation times using tributyrin as a substrate.

Table 1: Data Collection and Final Refinement Statistics

data collection	
resolution limit (Å)	20−2.8
completeness (%)	93.0 (81.8)
redundancy	3.4 (3.2)
R_{sym}[a]	5.4 (21.2)
$I/\sigma(I)$	12.3 (2.5)
refinement	
resolution limits (Å)	20−2.8
no. of reflections (test set)	21648 (1493)
no. of protein atoms	6064
no. of sugar atoms	112
no. of inhibitor atoms	36
no. of water molecules	220
final R_{factor}[b] (%)/R_{free}[c] (%)	20.4/24.9
B-factors (Å^2)	
protein	40.6
sugar	52.2
inhibitor	43.3
waters	38.5
rms deviations	
bonds (Å)	0.0073
angles (deg)	1.38
impropers (deg)	0.75
dihedrals (deg)	26.1

[a] $R_{sym} = \sum_h\sum_i|I_{hi} - \langle I_h\rangle|/\sum_h\sum_i I_{hi}$. [b] $R_{factor} = \sum_h||F_{obs}| - |F_{calc}||/\sum_h|F_{obs}|$, where F_{obs} and F_{calc} are the observed and calculated structure factor amplitudes, respectively. [c] R_{free} is calculated with 7% of the diffraction data, which were not used during the refinement.

Crystallization and X-ray Diffraction Studies. The crystallization conditions and the space group for the DGL−$C_{11}Y_4(-)$ complex are the same as those described for the DGL−$C_{11}Y_4(+)$ complex (*2*). The crystals belong to space group $C222_1$ (a = 62.7 Å, b = 167.1 Å, and c = 178.5 Å).

X-ray diffraction data were collected to 2.8 Å resolution on a Mar Research CDD camera with a λ of 0.9798 Å on beamline ID14 EH4 at ESRF. The data were processed using the DENZO software package (*21*). Specific volume calculations yielded two molecules per asymmetric unit, with a solvent content of 56%. A total number of 21 648 unique reflections were indexed using the SCALE pack (*20*) program with an R_{merge} on intensities of 5.4%, a data set multiplicity of 3.4, and a completeness of 93.1%, between 20.0 and 2.8 Å.

Determination of the Structure. The structure of the DGL−$C_{11}Y_4(-)$ complex was determined with the molecular replacement method using the AMoRe program (*22*). The structure of the DGL in complex with the (+) enantiomer [DGL−$C_{11}Y_4(+)$] (PDB entry 1K8Q) was used as the search model. The rotation function gave a unique solution, leading to two positions in the translation function. Before fitting was carried out, the correlation coefficient and R_{factor} were 41.8 and 43.5%, respectively, which refined to 48.2 and 40.4%, respectively. The $C_{11}Y_4(-)$ phosphonate enantiomer was built in the Fourier difference map with the program Turbo-Frodo (*23*). CNS refinement (*24*) was carried out between 20 and 2.8 Å resolution. The final model has good geometry, with an R_{free} of 24.9% and an R_{factor} of 20.4%. The statistics of the refinement are given in Table 1.

Modeling of the Alkyl Phosphonates in Complex with Gastric Lipases. A model was constructed for the open form

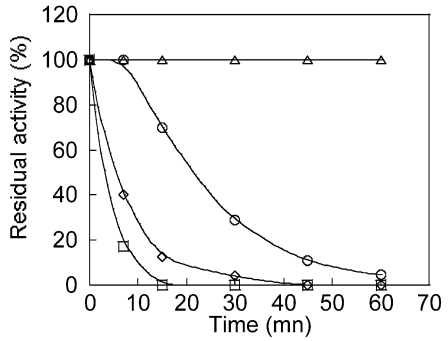

FIGURE 1: Kinetic curves of HGL inactivation by the $C_6Y_{11}(+)$ (○), $C_8Y_{11}(+)$ (□), $C_{12}Y_{11}(+)$ (◇), and $C_{16}Y_{11}(+)$ (△) phosphonates. The inhibitors were used at a molar excess of 50, in the presence of β-OG (see Experimental Procedures).

of HGL from the X-ray-determined open form of DGL. The residues were substituted manually with Turbo-Frodo, and amino acid side chain best fitting was performed with the rotamer search function. The molecule was then subjected to a minimization of the energy using the CNS software.

Both R_P and S_P enantiomers of phosphonates with an alkoxy chain of 11 carbon atoms and a variable alkyl chain length (from 6 to 16 carbons, $C_{6-16}Y_{11}$) were built in complex with DGL and HGL. Since the $C_{11}Y_4(+)$ in complex with DGL had an S_P absolute configuration, it was therefore used as a model for all the S_P enantiomers. Carbon atoms were added or deleted using Turbo-Frodo (*23*) to build $C_{6-16}Y_{11}(S_P)$ enantiomers, and a torsion was needed in the case of long alkyl/alkoxy chain phosphonates to avoid steric hindrance with side chain residues of the amino acids of the catalytic crevice. The phosphonate inhibitors were all kept covalently bound to the active site serine (Ser153). The lipase−inhibitor complexes were then subjected to energy minimization using the CNS software. The input topology and parameter files of the alkyl inhibitor and of the lipase were adapted from those used to refine the DGL−$C_{11}Y_4(+)$ complex crystal structure. Minimization of the DGL−inhibitor covalent complexes was carried out in two sequential steps, applying potential harmonic constants on the C_α atoms of 10 and 2 kcal mol^{-1} Å^{-2}, respectively. Ten thousand calculation steps were run in each minimization round.

The positions of the alkoxy and alkyl chains of the methyl undecyl phosphonate enantiomers were inverted in the active site of the HPL as previously performed by Egloff *et al.* (*15*). On the basis of these data, we have switched the alkyl and alkoxy chains of the S_P enantiomers to obtain the starting model for the R_P enantiomers. Then the R_P enantiomers, with variable chain lengths, were built, and minimization calculations were run as described for the S_P enantiomers.

The triglyceryl intermediate was modeled on the basis of the inhibitor starting position and adjusted manually. It was then subjected to energy minimization with CNS, with the same strategy that was used for the phosphonate inhibitors.

RESULTS AND DISCUSSION

Inhibition of Gastric Lipases by Various Alkyl Phosphonate Enantiomers. To study the enantio preference of gastric lipase toward phosphonate compounds with variable alkyl chain lengths, a series of (+) and (−) enantiomers were assayed as potential inhibitors of HGL (Figure 1) and DGL (Tables 2 and 3). Two series of inhibitors were used. The first series has an alkyl chain length varying from 6 to 16 carbon atoms and an 11-carbon alkoxy chain ($C_{6-16}Y_{11}$ alkyl phosphonates); the second series possesses an 11-carbon alkyl chain and an alkoxy chain with either four ($C_{11}Y_4$) or six ($C_{11}Y_6$) carbon atoms.

Table 2: Half-Lives (minutes) of the DGL Activity in the Presence of $C_{6-16}Y_{11}$ Enantiomers[a]

	β-OG (40 mM)		NaTDC (10 mM)	
inhibitor	inhibitor molar excess of 50	inhibitor molar excess of 500	inhibitor molar excess of 50	inhibitor molar excess of 500
$C_6Y_{11}(+)$	3.3	2	53	23.5
$C_8Y_{11}(+)$	3.3	3	99	36.4
$C_{12}Y_{11}(+)$	6	4.2	NI	48.2
$C_{16}Y_{11}(+)$	7	5.5	NI	65
$C_6Y_{11}(-)$	11	17	130	165
$C_8Y_{11}(-)$	5.3	7.5	130	143
$C_{12}Y_{11}(-)$	98	95	150	173
$C_{16}Y_{11}(-)$	123	123	140	161.8

[a] NI means no inhibition and corresponds to a residual lipase activity exceeding 90% after incubation for 60 min with the inhibitor. Experiments were performed at least twice, and the maximal standard error was 8% of the reported values.

The (+) enantiomers of $C_{6-16}Y_{11}$ alkyl phosphonates were found to be powerful inactivators of DGL, particularly in the presence of β-OG, since the time required to observe a loss of 50% of the initial lipase activity ($t_{1/2}$) did not exceed 7 min, at an inhibitor to lipase molar excess of 50 (Table 2). The inhibition is less efficient, however, in the presence of NaTDC since $t_{1/2}$ values were found to range between 53 min [$C_6Y_{11}(+)$] and 99 min [$C_8Y_{11}(+)$]. The $C_{12}Y_{11}(+)$ and $C_{16}Y_{11}(+)$ failed to inactivate DGL even in the presence of 50 mM NaTDC. From these data, it can also be concluded that the (−) enantiomers of $C_{6-16}Y_{11}$ exhibit a weaker capacity to inhibit DGL, even in the presence of β-OG or NaTDC.

The $C_{6-16}Y_{11}(+)$ enantiomers were also tested for their inhibitory capacity on HGL. The inhibitors with short (C_6 and C_8) and medium (C_{12}) alkyl chain lengths were found to be inhibitors with $t_{1/2}$ values of 4, 7, and 22 min for $C_8Y_{11}(+)$, $C_{12}Y_{11}(+)$, and $C_6Y_{11}(+)$, respectively. In contrast, long chain inhibitors such as $C_{16}Y_{11}(+)$ failed to inactivate HGL (Figure 1). These results agree with those obtained by Cavalier *et al.* (*25*) using the monolayer technique.

It seems that a relation was established between the order of the elution of the enantiomers from the chiral HPLC column and the inhibition properties of the phosphonate rather than their optical rotations. Indeed, the slowly eluted $C_{11}Y_4(-)$ as well as the $C_{11}Y_6(-)$ enantiomers were found to inactivate DGL more efficiently than the fastly eluted $C_{11}Y_4(+)$ and $C_{11}Y_6(+)$ do (Table 3). DGL lost half of its initial activity within 4, 3, 12, and 7.2 min with $C_{11}Y_4(-)$, $C_{11}Y_6(-)$, $C_{11}Y_4(+)$, and $C_{11}Y_6(+)$, respectively (Table 3). Interestingly, the $C_{11}Y_4$ and $C_{11}Y_6$ phosphonates are powerful DGL inactivators but affect to a lesser extent the HGL activity. As observed for the series of $C_{6-16}Y_{11}$ enantiomers, the inhibition rate is drastically accelerated in the presence of β-OG as compared to that in NaTDC (data not shown). It is worth noticing that comparable inhibition data were obtained when the $C_{6-16}Y_{11}(+)$, $C_{11}Y_4$, and $C_{11}Y_6$ alkyl phosphonate to lipase molar excess was 50 or 500 (Tables 2 and 3).

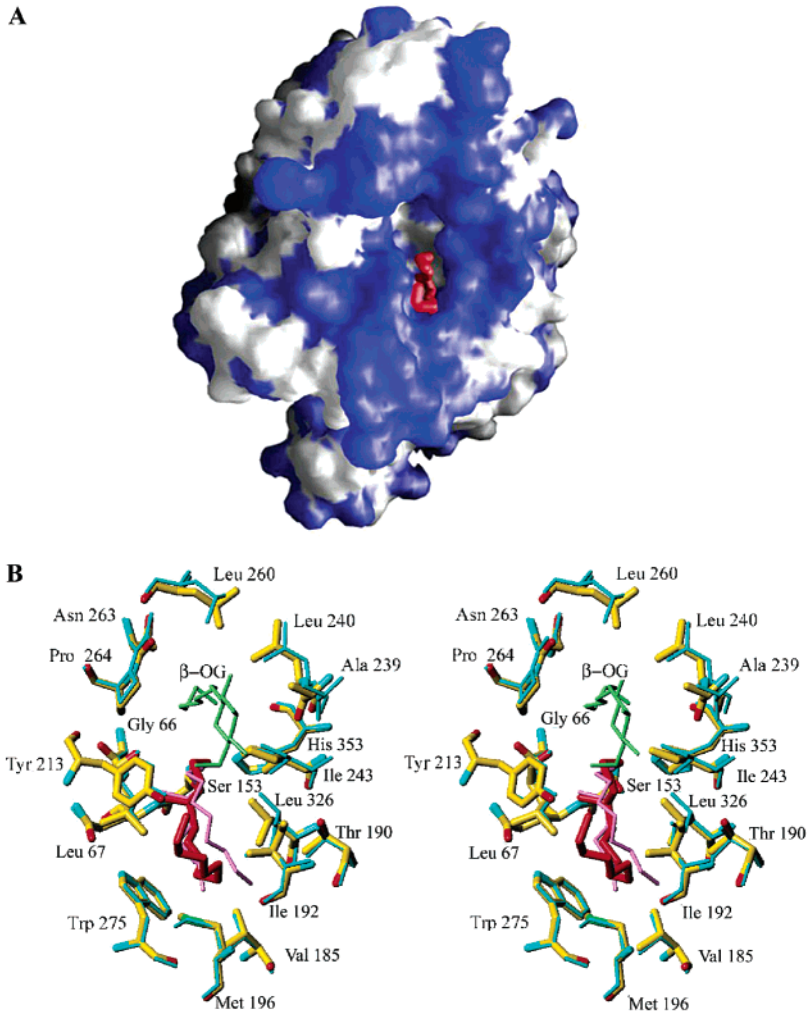

FIGURE 2: Views of the structure of DGL in complex with $C_{11}Y_4(-)$. (A) Solid representation of the complex. Hydrophobic residues are shown in blue, and the inhibitor is shown as red sticks. (B) Stereoview and superposition of the catalytic crevice of the DGL−$C_{11}Y_4(-)$ (red line) and DGL−$C_{11}Y_4(+)$ (thin pink line) complexes with a β-OG molecule (thin green line). Residues involved in the interaction with the phosphonate are represented as sticks.

Table 3: Half-Lives (minutes) of the DGL and HGL Activities in the Presence of $C_{11}Y_4$ or $C_{11}Y_6$ Enantiomers and β-OG (40 mM)[a]

	DGL		HGL	
inhibitor	inhibitor molar excess of 50	inhibitor molar excess of 500	inhibitor molar excess of 50	inhibitor molar excess of 500
$C_{11}Y_4(+)$	12	9.6	NI	NI
$C_{11}Y_6(+)$	7.2	5.3	63	76
$C_{11}Y_4(-)$	4	3.5	20	21
$C_{11}Y_6(-)$	3	3.5	19.5	19.5

[a] NI means no inhibition and corresponds to a residual lipase activity exceeding 90% after incubation for 60 min with the inhibitor. Experiments were performed at least twice, and the maximal standard error was 8% of the reported values.

Overall Structure of DGL in Complex with the (−) Enantiomer of $C_{11}Y_4$. We previously determined the three-dimensional structure of the open DGL in complex with the (+) enantiomer of $C_{11}Y_4$ [DGL−$C_{11}Y_4(+)$]. Crystals of the DGL in complex with the (−) enantiomer of $C_{11}Y_4$ [DGL−$C_{11}Y_4(-)$] were presently obtained under the same experimental conditions as previously described (*2*) and belong to the same crystal form. The crystal structure was determined at 2.8 Å resolution (Figure 2A). As previously described, the DGL molecule consists of an α/β core domain covered by cap and lid domains. No significant differences occur between the structures of the two DGL complexes since the rmsd between them is 0.2 Å. The crystal packing of the DGL molecule is similar in both complexes, and the observed glycosyl moieties are also identical.

The residues involved in the interaction with each enantiomer are located in a deep crevice that is ~20 Å × 20 Å × 7 Å (Figure 2B). The residues of the catalytic triad (Ser153, Asp324, and His353) and the oxyanion hole (Leu67 and Gln154) were indeed perfectly superimposable. A slight deviation of ~1 Å was observed, however, between the two lid domains (residues 212−251) and between two helices (residues 186−208) belonging to the cap domain. This region is probably involved in the interactions with the lipid substrate and exposes a patch of hydrophobic residues of 2800 Å^2. A leucine rich region (Leu68, -191, -195, -197, -234, -235, -260, and -326) could play a crucial role in the interactions with the lipid matrix.

Active Site-Bound Inhibitor. The $C_{11}Y_4(-)$ enantiomer was easily positioned in the electron density map, covalently bound to the catalytic serine. When both crystal structures are superimposed, the alkyl chain of one $C_{11}Y_4$ inhibitor enantiomer follows accurately the track of the ester chain of the other reverse optical enantiomer. Practically, the first

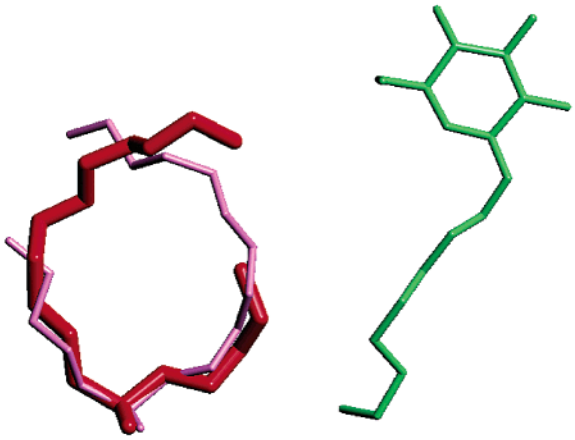

FIGURE 3: Superimposition of $C_{11}Y_4(+)$ (thin pink line) and $C_{11}Y_4(-)$ (thick red line) with a β-OG molecule (thin green line).

Table 4: (A) Correlation between the Optical Activity and the Absolute Configuration of the Phosphonate Inhibitor and (B) Scheme of the Nucleophilic Substitution of Ser153 on the Chiral Inhibitor Phosphonate Compound

(A) phosphonate optical enantiomer	absolute configuration	
	covalently bound	free
$C_{11}Y_4(-)$	R_P	S_P
$C_{11}Y_4(+)$	S_P	R_P

(B)

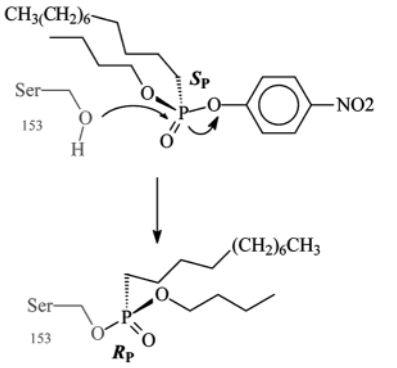

four carbons of the alkyl chain of the $C_{11}Y_4(-)$ enantiomer were aligned with the alkoxy chains of the $C_{11}Y_4(+)$ enantiomer (Figure 3), and the alkyl chain was further built, pointing toward the entry of the catalytic pocket (Figure 2A). Surprisingly, the β-OG molecule, previously observed stacking against the inhibitor in the active site of the DGL−$C_{11}Y_4(+)$ complex, is absent in the present DGL−$C_{11}Y_4(-)$ complex (Figure 2A). A spare electron density is observed in the active site, indicating that multiple conformations and/or agitated β-OG might also be present in this structure, but cannot be modeled in the electron density map.

From this crystal structure of the complex between DGL and the $C_{11}Y_4(-)$ inhibitor, we could unambiguously attribute the absolute R_P configuration to the phosphorus atom from the bound phosphonate. Since phosphonate inhibition proceeds by a nucleophilic attack from the catalytic serine on the phosphorus atom, through a SN2 mechanism with an inversion of configuration (see the reaction scheme from Table 4B), the original absolute configuration of the free inhibitors was reversed as compared to the covalently bound phosphonates. We can thus deduce that the free $C_{11}Y_4(-)$ molecule is the S_P enantiomer, and consequently, the free $C_{11}Y_4(+)$ molecule is its R_P antipod (Table 4A).

Table 5: Distances (Å) between Nϵ of the Catalytic Histidine (His353) and O_1 of the Phosphoester Bond As Deduced from the Models of the DGL−Phosphonate Complexes

	R_P enantiomeric configuration	S_P enantiomeric configuration
C_6Y_{11}	2.96	5.07
C_8Y_{11}	2.96	5.03
$C_{12}Y_{11}$	2.98	5.15
$C_{16}Y_{11}$	2.88	5.02
$C_{11}Y_4$	3.01	5.00

The most prominent structural feature is the stabilization of the most powerful inhibitor [$C_{11}Y_4(-)$] by a hydrogen bond (3.2 Å) between the O_1 atom of the phospho ester group and Nϵ of the catalytic histidine (His353). In the case of the less potent inhibitor [$C_{11}Y_4(+)$], the hydrogen bond is not possible since the interatomic distance is 4.5 Å. Likewise, a similar hydrogen bond between O_1 of the phosphonate inhibitors and the catalytic histidine was proposed to account for the enantio preference of *Candida rugosa* lipase toward the R_P enantiomer of menthyl esters (*11*) and *Pseudomonas cepacia* lipase toward the R_P triacylglycerol analogues (*9*).

Modeling of Alkyl Phosphonates in the Active Sites of Gastric Lipases. In an attempt to understand on a structural basis the stereospecificity of gastric lipases toward alkyl phosphonate inhibitors, we have modeled, inside the catalytic site of DGL and HGL, the binding of the two enantiomers of several phosphonate inhibitors for which inhibition data were available. Using the previous three-dimensional structure of the DGL inhibited by the $C_{11}Y_4(+)$ phosphonate, we have built models of S_P enantiomers of phosphonate inhibitors (S_P enantiomeric configuration) with variable alkyl chains ($C_{6-16}Y_{11}$), covalently bound to the catalytic serine. The β-OG molecule previously observed in the catalytic site was kept in the models. With regard to the enantiomeric antipod models of the covalently bound $C_{6-16}Y_{11}$ (R_P enantiomer configuration), we have switched the alkyl and alkoxy chains of $C_{11}Y_4$ in its S_P configuration and added or deleted atoms to obtain the required alkyl chain length. All the alkyl chains of the various enantiomers were found to fit nicely, without steric clash, inside the active site of DGL. There is space enough in the active site of DGL for a chain length of 10−12 carbon atoms. Consequently, all inhibitors with a chain length of fewer than 12 carbon atoms were found to be completely buried inside the catalytic crevice, whereas longer chains were found to point out of the cavity and would probably interact with the lipid matrix (Figure 4A). As observed in this crystal structure of the DGL−$C_{11}Y_4(-)$ complex, all the bound enantiomers in their R_P configuration were stabilized by a hydrogen bond with the catalytic histidine (Table 5). In contrast, this hydrogen bond was not established with the bound enantiomers with the S_P configuration, their O_1 atom being located more than 5 Å from the Nϵ atom of the catalytic histidine.

Since the sequences of HGL and DGL are 85.7% identical, a homology model of the open form of HGL was built up, based on the crystal structure of the DGL−$C_{11}Y_4(+)$ complex. Models of complexes of HGL with phosphonate inhibitors were also constructed as described previously for DGL. The results obtained with HGL and the two series of phosphonate enantiomers were comparable to those obtained with DGL. No apparent structural feature could explain the

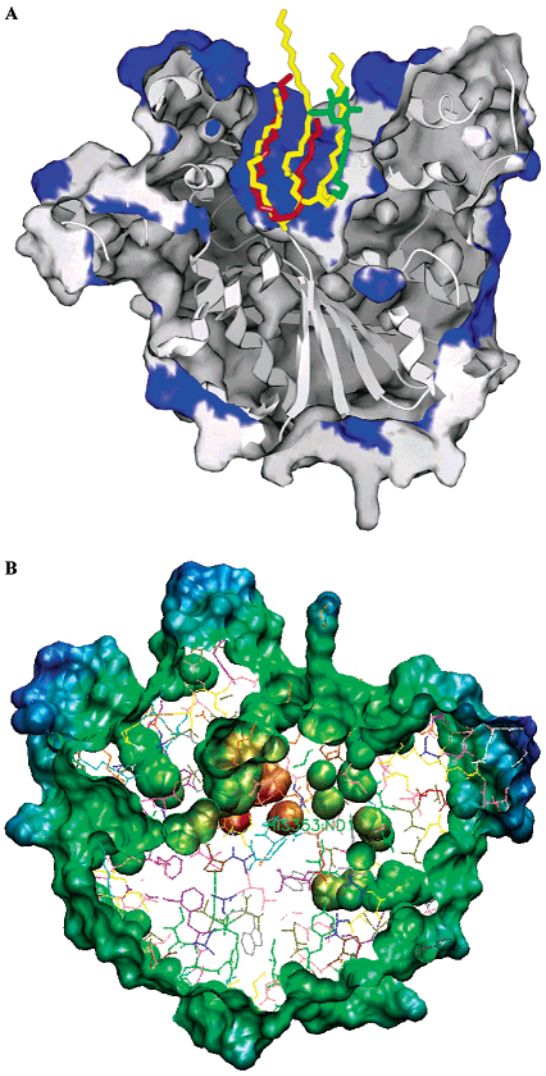

FIGURE 4: Superimposition of models of the $C_{16}Y_{11}$ (R_P configuration) inhibitor (red) and the first tetrahedral intermediate of a tristearoylglycerol molecule (yellow) inside the active site of DGL. (A) Solid representation of DGL with hydrophobic residues shown in blue. The inhibitor (red stick) and the β-OG molecule (green stick) as well as the triglyceride molecule (yellow) show no steric hindrance with the surface of the lipase. The β-OG molecule observed in the active site was maintained during the calculations. The distal carbon atoms of the chains are pointing toward the solvent, with both the phosphonate and the triglyceryl intermediate. (B) Slabbed surface of the DGL−triglyceryl intermediate model showing the water access channel to the active site (arrows).

better inhibition of the phosphonates toward DGL as compared to HGL, however (Table 3).

Model of a Triacylglycerol in the Active Site of Gastric Lipases. The modeling of the covalently bound phosphonate inhibitors inside the active site of the gastric lipases and the stabilization by a hydrogen bond of the compounds with an R_P configuration prompted us to establish a model for a long chain triacylglycerol intermediate bound in the active site of the DGL. We built the first tetrahedral intermediate corresponding to the tristearoyl−lipase complex by aligning two adjacent chains of the triacylglycerol with the alkyl and alkoxy chains of the $C_{11}Y_4$ molecule and keeping it within hydrogen bonding distance of the catalytic histidine. Under these conditions, the triglyceride intermediate fills completely the active site crevice of DGL (Figure 4A). A total of 634 Å^2 of the DGL water accessible surface is covered by the triglyceride, revealing that no room is available for any molecule to squeeze inside the active site when the tetrahedral intermediate is bound. The same model was carried out with HGL (data not shown), leading to similar results. However, although the alkyl chains exhibit some slight positional differences between DGL and HGL (data not shown), they do not explain the marked preference of DGL for long chain triacylglycerol as compared to HGL (*26*).

The shielding of the active site by the bound intermediate seems to be a specific feature of gastric lipases in contrast with pancreatic lipases which possess a much more accessible active site. Lipases being hydrolases, they need rapid access of water to the catalytic triad to hydrolyze efficiently the first tetrahaedral intermediate (in DGL at a rate of ~1000 s^{-1}). Clearly, access of water to the gastric lipase active site seems to be drastically hindered considering both the lipase adsorption to the lipidic interface and the penetration of the substrate into the active site crevice. In similar situations with several hydrolases, a channel distinct from the active site could be identified for supplying it with a flux of water molecules (*27*). Such a water channel can be identified in DGL by observing its water accessible surface (Figure 4B).

ACKNOWLEDGMENT

We thank Dr. Jean-François Cavalier (ENSSPICAM) for the chemical synthesis and his generous gifts of the phosphonate inhibitors. We are particularly indebted to Dr. Charles Danzin and Dr. Patrick Berna (Jouveinal/Parke-Davis) for their generous gift of r-DGL samples. We are grateful to our colleague Dr. Véronique Gruber at Meristem Therapeutics for technical assistance and contribution to DGL gene cloning, transformation, and production of maize seeds. Sylvie Dufour and Carole Bloës (Jouveinal/Parke-Davis) are thanked for their technical assistance in the r-DGL purification. We thank ESRF for beamtime allocation. We are grateful to Frédéric Carrière for helpful discussions and for his constant interest in this topic. We also thank Dr. Jessica Blanc for correcting the English.

REFERENCES

1. Roussel, A., Canaan, S., Egloff, M., Riviere, M., Dupuis, L., Verger, R., and Cambillau, C. (1999) *J. Biol. Chem. 274*, 16995−17002.
2. Roussel, A., Miled, N., Berti-Dupuis, L., Riviere, M., Spinelli, S., Berna, P., Gruber, V., Verger, R., and Cambillau, C. (2002) *J. Biol. Chem. 277*, 2266−2274.
3. Yu, L., and Dennis, E. A. (1991) *Proc. Natl. Acad. Sci. U.S.A. 88*, 9325−9329.
4. Yuan, W., Quinn, D. M., Sigler, P. B., and Gelb, M. H. (1990) *Biochemistry 29*, 6082−6094.
5. Björkling, F., Dahl, A., Patkar, S., and Zundel, M. (1994) *Bioorg. Med. Chem. 2*, 697−705.
6. Moreau, H., Moulin, A., Gargouri, Y., Noël, J.-P., and Verger, R. (1991) *Biochemistry 30*, 1037−1041.
7. Patkar, S., and Björkling, F. (1994) in *Lipases. Their structure, biochemistry and application* (Wooley, P., and Petersen, S. B., Eds.) pp 207−224, Cambridge University Press, Cambridge, U.K.
8. Marguet, F., Cudrey, C., Verger, R., and Buono, G. (1994) *Biochim. Biophys. Acta 1210*, 157−166.
9. Lang, D., Mannesse, M., de Haas, G., Verheij, H., and Dijkstra, B. (1998) *Eur. J. Biochem. 254* (2), 333−340.
10. Cavalier, J. F., Ransac, S., Verger, R., and Buono, G. (1999) *Chem. Phys. Lipids 100*, 3−31.
11. Cygler, M., Grochulski, P., Kazlauskas, R. J., Schrag, J. D., Bouthillier, F., Rubin, B., Serreqi, A. N., and Gupta, A. K. (1994) *J. Am. Chem. Soc. 116*, 3180−3186.

12. Derewenda, U., Brzozowski, A. M., Lawson, D. M., and Derewenda, Z. S. (1992) *Biochemistry 31*, 1532−1541.
13. Brzozowski, A. M., Derewenda, U., Derewenda, Z. S., Dodson, G. G., Lawson, D. M., Turkenburg, J. P., Bjorkling, F., Huge-Jensen, B., Patkar, S. A., and Thim, L. (1991) *Nature 351*, 491−494.
14. Cygler, M., Grochulski, P., Li, Y., Schrag, J. D., Bouthillier, F., Smith, P., Harrison, D., and Rubin, B. (1992) Lipase: Structure, Mechanism and Genetic Engineering, October 1−3, Capri, Italy.
15. Egloff, M.-P., Marguet, F., Buono, G., Verger, R., Cambillau, C., and van Tilbeurgh, H. (1995) *Biochemistry 34*, 2751−2762.
16. Desnuelle, P., Sarda, L., and Ailhaud, G. (1960) *Biochim. Biophys. Acta 37*, 570−571.
17. Maylié, M. F., Charles, M., and Desnuelle, P. (1972) *Biochim. Biophys. Acta 276*, 162−175.
18. Rouard, M., Sari, H., Nurit, S., Entressangles, B., and Desnuelle, P. (1978) *Biochim. Biophys. Acta 530*, 227−235.
19. Canaan, S., Dupuis, L., Rivière, M., Faessel, K., Romette, J. L., Verger, R., and Wicker-Planquart, C. (1998) *Protein Expression Purif. 14*, 23−30.
20. Gargouri, Y., Piéroni, G., Rivière, C., Saunière, J.-F., Lowe, P. A., Sarda, L., and Verger, R. (1986) *Gastroenterology 91*, 919−925.
21. Otwinovsky, Z. (1993) *DENZO*, Yale University, New Haven, CT.
22. Navaza, J. (1994) *Acta Crystallogr. A50*, 157−163.
23. Roussel, A., and Cambillau, C. (1991) in *Silicon Graphics Geometry Partners Directory*, pp 86, Silicon Graphics, Mountain View, CA.
24. Brünger, A. T., Adams, P. D., Clore, G. M., DeLano, W. L., Gros, P., Grosse-Kunstleve, R. W., Jiang, J. S., Kuszewski, J., Nilges, M., Pannu, N. S., Read, R. J., Rice, L. M., Simonson, T., and Warren, G. L. (1998) *Acta Crystallogr. D54*, 905−921.
25. Cavalier, J., Buono, G., and Verger, R. (2000) *Acc. Chem. Res. 33*, 579−589.
26. Carrière, F., Moreau, H., Raphel, V., Laugier, R., Bénicourt, C., Junien, J.-L., and Verger, R. (1991) *Eur. J. Biochem. 202*, 75−83.
27. Wendt, K., Lenhart, A., and Schulz, G. (1999) *J. Mol. Biol. 286*, 175−187.

BI034964P